A novel vision-based system for analysis of abdominal aortic aneurysm

ANDRZEJ POLANCZYK[1*], MACIEJ POLANCZYK[1], MICHAL PODGÓRSKI[2], ALEKSANDRA PIECHOTA-POLANCZYK[3]
[1] Department of Heat and Mass Transfer, Faculty of Process and Environmental Engineering, Lodz University of Technology, Lodz, POLAND
[2] Polish Mother's Memorial Hospital Research Institute, POLAND
[3] Department of Medical Biotechnology, Faculty of Biochemistry, Biophysics and Biotechnology, Jagiellonian University, Krakow, POLAND
andrzej.polanczyk@gmail.com

Abstract: - Aortic aneurysm weakens the vessel wall and significantly changes blood hemodynamics. We proposed a novel Vision-Based- System (VBS) for the analysis of abdominal aortic aneurysm (AAA) wall deformation for different hemodynamic conditions. The VBS system has hardware part composed of 9 cameras system built around a transparent container filled with liquid and surrounding a 3d model of aorta, thus simulating work of aorta in human's body. While, software part is based on self-made algorithm for the analysis of captured images by the set of cameras and calculation of wall deformation factor which can be assessed by physicians. The most effort was allocated into image rectification and tracking aorta size in sequence of images. To verify the VBS a series of experiments were performed with the use of 3d-printed elastic AAA models from three patients for the reconstruction of real hemodynamic. Experimental results were confronted with medical data from AngioCT and 2D speckle-tracking echocardiography (2DSTE). The accuracy of the proposed method for the reconstruction of the AAA deformation after comparison with expert assessment (clinician) was 98.56%. We demonstrated that there is a range between cameras and container in which correct results can be acquired, without influence of light refraction. Correct recognition of spatial configuration of the AAA and the deformation of its wall is one of the key points in the surgical treatment. Mistakes made at this stage may lead to re-surgical operations which is unnecessary risk for patients' lives.

Key-Words: Deformation measurement, Non-contact optical strain testing, Displacement measurement

1 Introduction

Aortic aneurysm weakens the vessel's wall and significantly changes blood hemodynamics [1]. The number of patients with diagnosed abdominal aortic aneurysm (AAA) is still increasing, concerning 5% of patients over 65 years of age. The AAA treatment depends on its diameter. When it is lower than 40 mm pharmacological treatment is applied, while the AAA with diameter equal or above 55 mm or growth rate over 5 mm every 6 months requires surgical repair either open or endovascular [2].

In clinical diagnostics, description of AAA's spatial configuration and its wall deformation indicates a combination of different techniques, e.g. echocardiography [3], 4D-US strain [4] or ultrasonography [5]. However, these techniques do not provide a real-time information, while collected raw data require postprocessing with dedicated software. On the contrary to *in-vivo* examination there are *ex-vivo* approaches basing on artificial models of AAA, e.g. silicon model connected with pulsatile artificial circulatory system [6]. Such approach enables application of optical methods supporting or replacing ultrasound examination. One of the non-contact optical methods applied in image processing is Digital Image Correlation (DIC) used for the measurement of changes in analyzed images [7, 8]. This technique may be applied for determination of object deformation [9-11], object displacement [12-14], and object strain [15, 16]. According to the development of image acquisition market and decreasing costs of production potential use of DIC technique is still increasing, e.g. mechanical testing applications [17-19], biology [20, 21], or art [22]. Therefore, the aim of this work was to prepare and validate a Vision Based System (VBS) for the analysis of the shape of a 3d elastic AAA model for different physiological and pathological conditions.

2.1 Medical data

With the use of medical data from AngioCT examination (GE Light-Speed 64 VCT; GE Healthcare, Fairfield, CT, USA) of three male patients and 3DDoctor software (Able Software Corp., Lexington, MA, USA) 3d geometries of the AAA's were reconstructed (Fig.1). The procedure

was thoroughly described in our previous paper [23]. Patients' data were retrospectively collected based on written informed consent. All medical data and images were anonymized by coding information before assessment and analysis. The study protocol was approved by the local ethics committee on the Medical University of Lodz (RNN/126/07/KE).

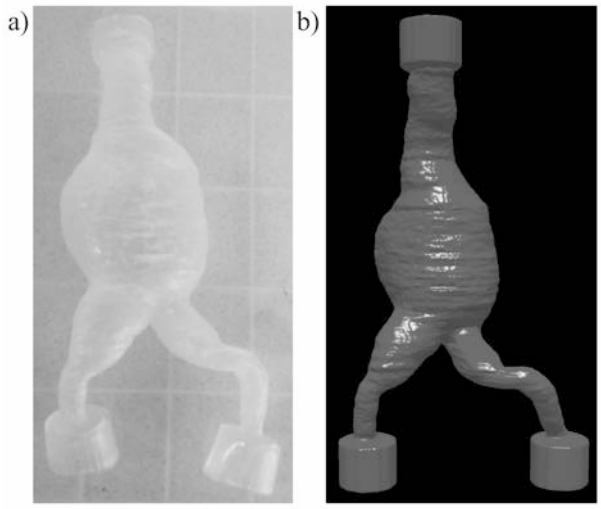

Fig.1 An example of AAA model: a) a 3d elastic model of printed AAA and b) a 3d virtual model of AAA.

Each time 3d elastic model of aorta was prepared with the use of 3d printing technique (3D printer, Object Eden 350, USA) and Tango Plus material (tensile strength 0.8-1.5 MPa, elongation at break 170-220%, compressive set 4-5%, shore hardness 26-28 scale A, tensile tear resistance 2-4 kg/cm, polymerized density 1.12-1.13 g/cm^3).

For the real hemodynamic reconstruction, the ECG trace from each patient was analyzed to measure the heart rate and applied as inlet boundary condition for the particular 3d elastic model of AAA. The procedure was described in details in our previous paper [24]. Data from ECG trace was implemented in self-constructed electric impulse generator which was able to regulate the pump pulsations. For every analyzed camera's angle one set of 10 cycles of contraction and relaxation was recorded.

2.2 Experimental set-up

A system of nine cameras of the same type (Full HD, resolution: 1920 x 1080, frame rate - 30 frames per second) was designed and combined in one set to analyze 3d models of AAA for different clinical conditions. Cameras were placed on a dedicated circular construction that allowed maintain constant distance between each two cameras (40 deg.) and the distance from the camera's lens to the middle point of the container (0.4m), where AAA models were placed.

To make analyzed object and applied algorithms independent from external light, a dedicated set of artificial light (LED technique) was designed and combined with the VBS. This operation allowed to achieve the same conditions of measurement for different time of day. Moreover, a set of cameras was placed in the parallel position to the floor to provide capability of horizontal movement. Due to the construction of a container, where AAA models were placed, with corners from aluminum profiles (thick 0.03m) obscuring a part of AAA models, not all angels were proper to record. Therefore, we had to modify a set of cameras in the way that each of them was able to move with 10 deg. step in both sides in the range of 40 deg.

A set of cameras was combined with portable working station Dell Precision M6400 with parameters as follow: four core Intel CPU (2.4GHz), 4GB RAM (1333MHz) Memory and Hard Drive 500 GB SSD.

2.3 Camera calibration

In the first step the calibration of a set of cameras in the VBS was obligatory. The mathematical algorithm prepared for the cameras' calibration enabled matrix of coefficients describing cameras' physical parameters (e.g. camera's focal length and image center) and distortions parameters estimation [25]. In the next step the coefficients matrix was applied in the image analysis stage to undistort images data captured with the set of cameras during acquisition stage [26, 27]. To describe the relation in coordinate system between object points of physical 3d geometry of the AAA and their projection into the image plane a Pinhole camera model was applied [28, 29]. A linear projection of 3d geometry of AAA points into the image plane was assumed. Implemented solution eliminated radial and tangential distortion [30]. Therefore, barrel, pincushion or tangential distortion effects was avoided (Fig.2).

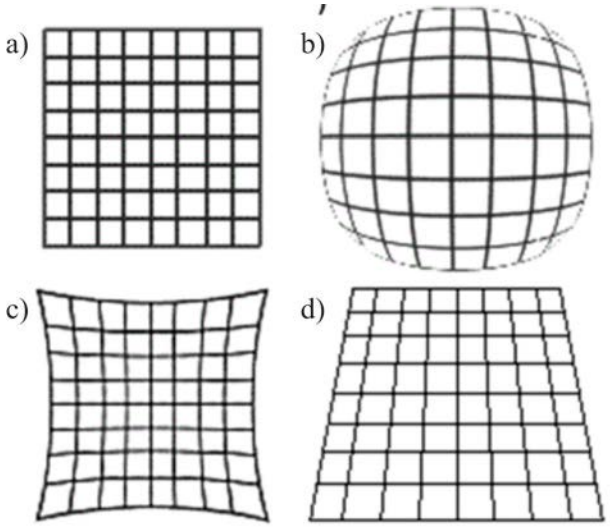

Fig. 2 An example of image distortions which may occur during data acquisition with a digital camera: a) no distortions b) barrel effect c) pincushion effect d) tangential distortion effect

2.3 Image acquisition

In the next step the mathematical algorithm for the image acquisition was prepared. The "producer - consumer" procedure was applied [31]. The architecture of procedure was as follow: (1) Capturing Images Thread (producer thread) (Fig.3), (2) Saving Images Thread (the first consumer thread) (Fig.4), (3) Previewing Images Thread (the second consumer thread) (Fig.5).

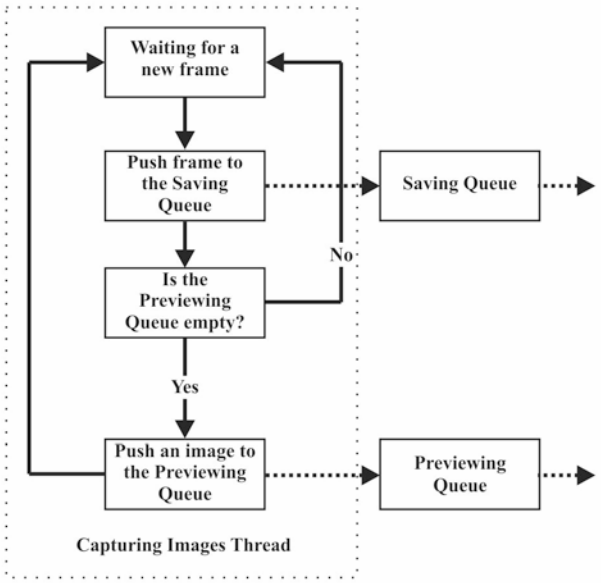

Fig. 3 Block diagram of Capturing Images Thread used in the VBS system.

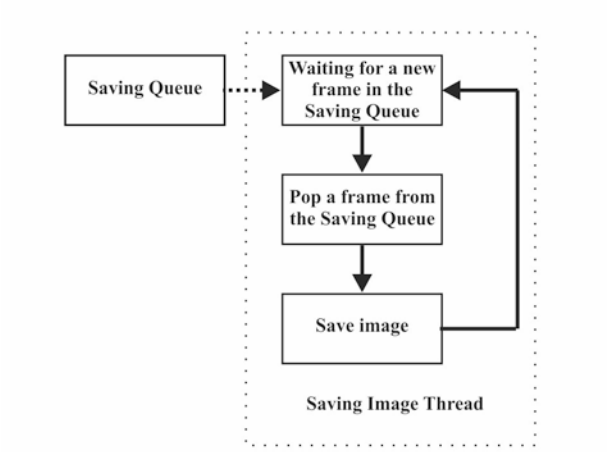

Fig. 4 Block diagram of Saving Images Thread used in the VBS system.

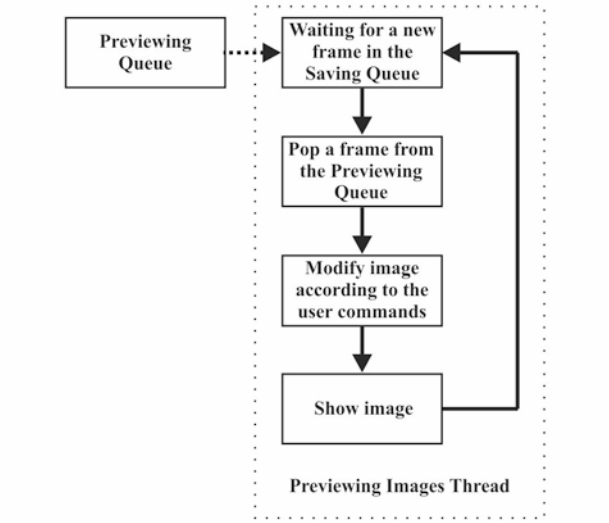

Fig. 5 Block diagram of Previewing Images Thread used in the VBS system.

The Capturing Images Thread (1) (Fig.3) was responsible for the process of collecting frames by the cameras and assigning them into two queues (saving queue and previewing queue) allocated in the memory. The first queue was consumed by the Saving Images Thread (2) (Fig.4). While, the second queue was consumed by the Previewing Images Thread (3) (Fig.5). As the Capturing Images Thread had the highest priority (it was obligatory for the operating system to allow this thread to work whenever it needs) it could combine all the images produced by the cameras with their highest frame rate. Moreover, the Capturing Images Thread did not consume much CPU. Therefore, it only forwarded the frames from cameras to the queues and then was suspended until another frame appears.

The Saving Images Thread (2) (Fig.4) was responsible for the popping frames from the saving

queue to allocate them on the hard disc. As the performance of the hard disc was unpredictable, and it was obligatory to save all frames immediately when the Saving Images Thread got access. This indicated to collect all frames in the queue limited only by the maximum size of the computer memory avoiding the situation when only one frame per second (or even less) would be saved instead of 30 frames per second necessary for further analysis. The priority level for the Saving Images Thread was one step lower compare to the Capturing Images Thread.

The Previewing Images Thread (3) (Fig.5) was responsible for the following elements: showing collected images and interaction with the user. The size of a queue in this thread was limited to the one image. It was necessary to avoid the situation when the user could select different view modes and affect a lot of CPU consumption. Therefore, it could pop frames from the preview queue slower than the Capturing Images Thread would be able to assign them to the queue. This would affect that the user would see images with a few seconds delay. Moreover, there appears no need for the user to check all the collected frames by the camera in the real time. The main point is to check the current image. Therefore, a low frame rate of showing images did not affect any issues.

Moreover, there appeared no dangers for the one image to be pushed by another image in the Capturing Images Thread. Unless, the Previewing Images Thread would take the image from the previewing queue to process it and show it to the user. Capturing Images Thread ignores pushing new images into previewing queue unless, the Previewing Images Thread would take the image from the previewing queue to process it and show it to the user. As the Previewing Images Thread had the highest CPU consumption it had assigned the lowest priority.

2.4 Image analysis

In the last step image analysis algorithm for the wall deformation of the AAA model for different clinical conditions was processed. As the long time was needed for analysis of the collected images, this step was set to work offline, after all necessary images were processed in previous algorithms. Four steps were performed in the process of image analysis: (1) image rectification, (2) image segmentation, (3) contour search, (4) aorta shape deformation factor calculation.

Since each collected image contained distortion, a rectification process with the use of coefficients from camera calibration was applied. Next, image segmentation was used. Application of segmentation process indicated that images should fulfil three criteria. First, collected image was present in grey color space, (2) image of aorta should be bright for the process of contour searching, (3) the rest of the image should be dark. By maintain of the light conditions during acquisition process the threshold value was adjusted. As a result of a segmentation process a binary image was produced. According to this aorta was represented with 1 and background was represented with 0. Finally, for the estimation of aorta's shape deformation factor (eq. 1) was applied.

$$\eta_i = \frac{F_{ic}}{F_c} \tag{1}$$

where,

F_{ic} - is the field size in the i-th image from c-th camera,

F_c - is the field size in reference image from c-th camera.

Aorta size was estimated as a field of points inside the recognized contour (Fig.6). Each result was compared to the size of the reference image. While, the reference image was defined as the first image in the sequence, performing motionless aorta for the camera's angles. Moreover, the ratio of the wall deformation was performed in the summary output file.

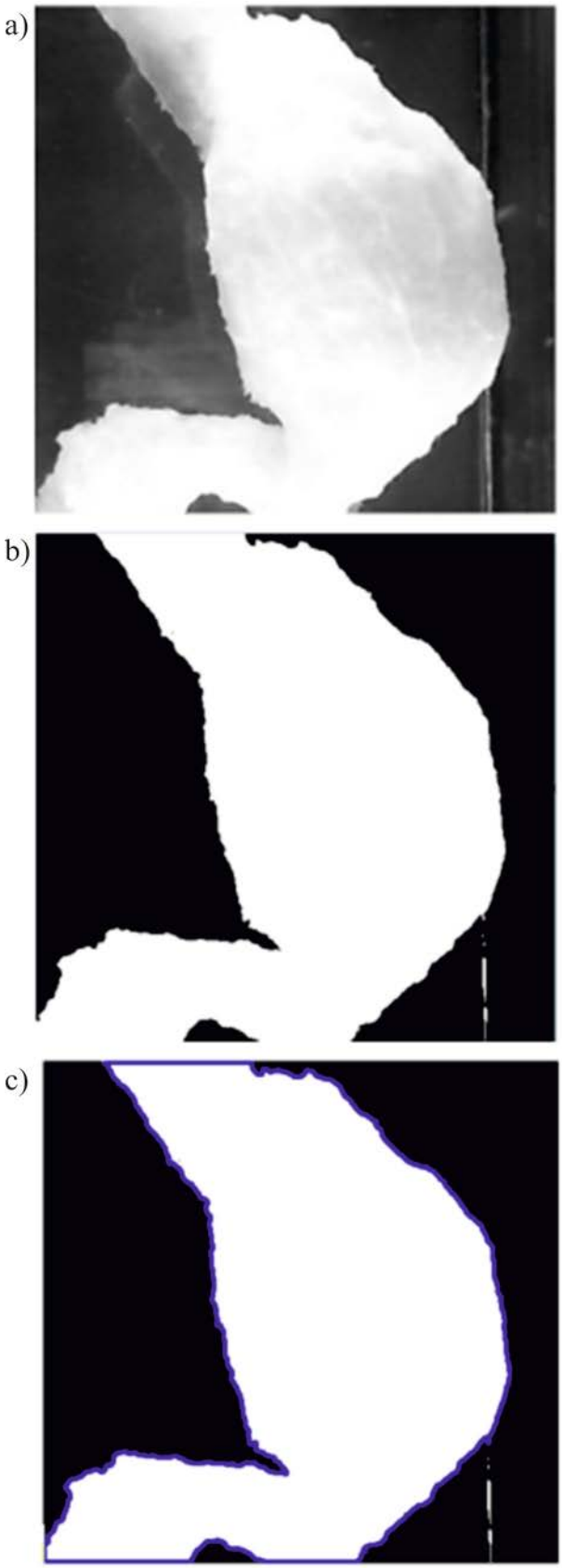

Fig.6 An example of AAA model images gathered during processing step: a) Image before segmentation b) Image after segmentation c) Contour detected (blue lines).

2.5 System verification

Two 2d different size squares with the specified dimensions (0.05 x 0.05m and 0.10 x 0.10m) were applied for the process of the verification. Squares were placed one by one inside the container which was empty or filled with the distilled water. This approach allowed objects deformation analysis. To eliminate the influence of distance between the analyzed objects and the camera's lens, variable position of squares (0.40m, 0.35m, 0.30m) from the lens, were analyzed. Furthermore, this allowed to control the description process of the analyzed objects in the time by the implemented algorithm.

Next, the deformation ratio as a difference between the recorded surfaces of the smaller or the bigger square was computed. This allowed to analyze average deformation recorded by the set of cameras and simulate the situation of the deformation of an irregular aneurysm sac wall. Optimal value of the ratio of the deformation for the specified dimensions of the analyzed squares was equal to 4. Moreover, as the shape of AAA model is not symmetric and the distance of each point of the AAA's wall to the container's wall is different it was obligatory to perform tests for the different position of the squares.

2.6 Statistical analysis

Statistical analysis was performed using Statistica 12 software. Values were presented as average wall deformation +/- standard deviation (SD).

3 Results

In our study we analyzed a VBS for three-dimensional reconstruction of wall deformation around 3d elastic AAA model.

Firstly, a verification of VBS was performed. 220 examinations were conducted for the squares 0.05 x 0.05m and 0.10 x 0.10m from different distance and in different environment (container empty and filled with the distilled water). After 220 experiments, half in empty container and half in container filled with distilled water, obtained results were comparable. For the squares placed in the empty container the average error was equal to 7.84±0.078% compare to the case with container filled with distilled water the average error was equal to 5.43±0.054%. The results indicate proper reflection of analyzed shapes in different environment.

After, initial verification of a system artificial models of the AAA for different flow conditions

(for three frequencies of flow pulsation: 60 min^{-1}, 70 min^{-1} and 100 min^{-1}) were analyzed. As the shape of aneurysm sac wall was not uniform and different values of deformation were recorded for different angles (Fig.7).

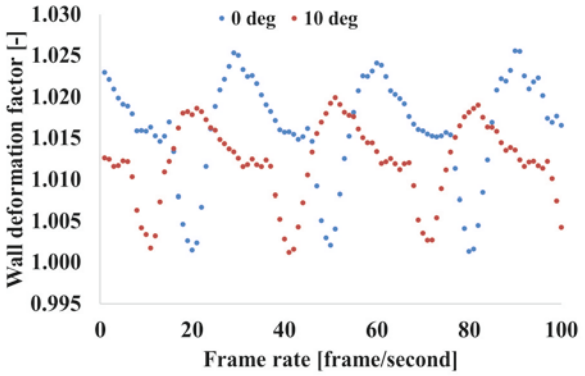

Fig.7 An example of acquisition of aneurysm sac wall deformation for 2 angles of camera position (0 and 10 deg.) in function of time for the frequency of flow pulsation 60 per minute and camera frame rate 30 frames per second.

Fig.8 presents average aneurysm sac wall deformation for the frequency of flow pulsation 60 min^{-1} and 70 ml per heart rate. Results indicated that self-made algorithm can reconstruct of 3d pulsation of aneurysm sac wall.

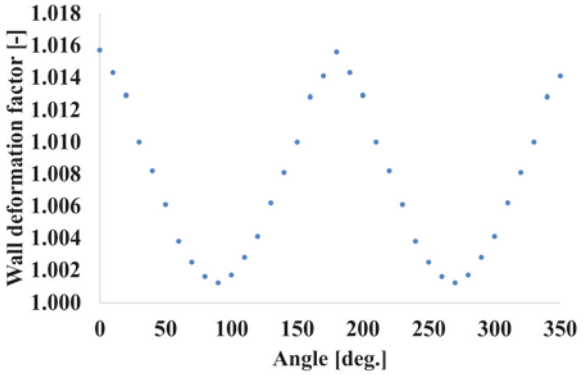

Fig.8 An example of average sac wall deformation for 70ml injection and frequency of pulsation 60min^{-1} calculated with a proposed self-made algorithm.

Depending on the analyzed point and the spatial configuration of AAA model the average deformation for the frequency of 60 min^{-1} was equal to 3.1±0.23% and to 10.3±0.3% for the smallest and highest wall pulsation, respectively. Average value of wall deformation for all three models was equal to 6.07±0.11%. Moreover, it was noticed that deformation of the AAA wall increased with rising frequency of flow pulsation. For the frequency of pulsation equal to 72 min^{-1} average wall deformation was in range 4.9±0.41% to 11.7±0.12%. While for the frequency of pulsation equal to 100 min^{-1} average wall deformation was in range 6.4±0.13% to 13.1±0.81%.

Finally, the experimental results were compared to the clinical data from the analyzed patient. Three frequency of flow pulsation were analyzed, e.g. 60 min^{-1}, 72 min^{-1} and 100 min^{-1}. For the frequency of flow pulsation equal to 60 min^{-1} average value of wall deformation for all three aneurysm sacs was equal to 5.86±0.23% (error was equal to 3.58%). Moreover, similarly to the experimental results it was noticed that an increase of the frequency of flow pulsation lead to an increase of aneurysm sac wall deformation. For the frequency of pulsation equal to 72 min^{-1} average value of wall deformation for all three aneurysms sac was equal to 9.21±0.05% (error was equal to 2.49%). While for the frequency of flow pulsation equal to 100 min^{-1} average value of wall deformation for whole model was equal to 10.53±0.31% (error was equal to 4.65%).

4 Conclusion

Our newly designed method, which combines application of 3d printed AAA models and optical methods, allows for detailed analysis of aneurysm sac wall mechanics in *ex-vivo* conditions. This may be further developing improve treatment strategies of patients with AAA. Potential implications comprise prediction of risk of aneurysm wall rupture and determining the weakest portion of wall. Moreover, verified *ex-vivo* analysis instead of *in-vivo* tests exclude the risk of patient injured or death, providing high quality results.

Acknowledgment

This work was supported by the Polish National Centre for Research and Development (501/10-34-19-605 to AP). Faculty of Biochemistry, Biophysics and Biotechnology of Jagiellonian University is a partner of the Leading National Research Center (KNOW) supported by the Ministry of Science and Higher Education.

References:

[1] C. W. Hicks, T. Obeid, I. Arhuidese, U. Qazi and M. B. Malas, Abdominal aortic aneurysm repair in octogenarians is associated with higher mortality compared with nonoctogenarians, *Journal of vascular surgery*, 64, 4, 2016, pp. 956-965 e1.

[2] R. M. Greenhalgh and J. T. Powell, Endovascular repair of abdominal aortic

aneurysm, *The New England journal of medicine*, 358, 5, 2008, pp. 494-501.

[3] B. M. Fadel, H. Bakarman, M. Al-Admawi, O. Bech-Hanssen and G. Di Salvo, Pulse-wave Doppler interrogation of the abdominal aorta: a window to the left heart and vasculature, *Echocardiography*, 31, 4, 2014, pp. 543-7.

[4] W. Derwich, A. Wittek, K. Pfister, K. Nelson, J. Bereiter-Hahn, C. P. Fritzen, C. Blase and T. Schmitz-Rixen, High Resolution Strain Analysis Comparing Aorta and Abdominal Aortic Aneurysm with Real Time Three Dimensional Speckle Tracking Ultrasound, *European journal of vascular and endovascular surgery : the official journal of the European Society for Vascular Surgery*, 51, 2, 2016, pp. 187-93.

[5] K. Karatolios, A. Wittek, T. H. Nwe, P. Bihari, A. Shelke, D. Josef, T. Schmitz-Rixen, J. Geks, B. Maisch, C. Blase, R. Moosdorf and S. Vogt, Method for aortic wall strain measurement with three-dimensional ultrasound speckle tracking and fitted finite element analysis, *The Annals of thoracic surgery*, 96, 5, 2013, pp. 1664-71.

[6] P. Bihari, A. Shelke, T. H. Nwe, M. Mularczyk, K. Nelson, T. Schmandra, P. Knez and T. Schmitz-Rixen, Strain measurement of abdominal aortic aneurysm with real-time 3D ultrasound speckle tracking, *European journal of vascular and endovascular surgery : the official journal of the European Society for Vascular Surgery*, 45, 4, 2013, pp. 315-23.

[7] W. H. Peters and W. F. Ranson, Digital imaging techniques in experimental stress analysis, *Opt. Eng.*, 3, 21, 1981, pp. 6.

[8] M. A. Sutton, W. J. Wolters, W. H. Peters, W. F. Ranson and S. R. McNeill, Determination of displacements using an improved digital correlation method., *Image Vis. Comput.*, 1, 3, 1983, pp.

[10] Bing Pan and Kai Li, A fast digital image correlation method for deformation measurement, *Optics and Lasers in Engineering*, 49, 7, 2011, pp. 7.

[11] B. Pan, Z. Wang and Z. Lu, Genuine full-field deformation measurement of an object with complex shape using reliability-guided digital image correlation, *Optics express*, 18, 2, 2010, pp. 1011-23.

[9] M. A. Sutton, Digital Image Correlation for Shape and Deformation Measurements, *Springer Handbook of Experimental Solid Mechanics*, Part C, 2008, pp. 36.

[13] B. Pan, K. M. Qian, H. M. Xie and A. SAsundi, Two-dimensional Digital Image Correlation for In-plane Displacement and Strain Measurement: A Review, *Measurement Science and Technology*, 20, 6, 2009, pp.

[12] B. Pan, Reliability-guided digital image correlation for image deformation measurement, *Applied optics*, 48, 8, 2009, pp. 1535-42.

[14] J. T. Ruan, F. Aymerich, W. Tong and Z. Y. Wang, Optical Evaluation on Delamination *Buckling* of Composite Laminate with Impact Damage, *Advances in Materials Science and Engineering*, 2014, 9, 2014, pp.

[17] T. Hua, H. Xie, B. Pan, Q. Wang and F. Dai, A new mark shearing technique for strain measurement *using* digital image correlation method, *The Review of scientific instruments*, 79, 10, 2008, pp. 105101.

[16] P. C. Hung and A. S. Voloshin, In-plane Strain Measurement by Digital Image Correlation, *J. of the Braz. Soc. of Mech. Sci. & Eng.*, 25, 3, 2003, pp. 215-221.

[20] S. H. Daly, Digital Image Correlation in Experimental Mechanics for Aerospace Materials and *Structures*, *Experimental Techniques for Structural Mechanics*, 10.1002/9780470686652.eae542, 2010, pp. Published Online: 15 DEC 2010.

[18] M. Malesa, K. Malowany, U. Tomczak, B. Siwek, M. Kujawinska and A. Sieminska-Lewandowska, Application of 3D digital image correlation in maintenance and process control in industry, *Computers in Industry*, 64, 9, 2013, pp. 1301-1315.

[19] J.-W. Zhou, D.-H. Liu, L.-Y. Shao and Z.-L. Wang, Application of Digital Image Correlation to Measurement of Packaging Material Mechanical Properties, *Mathematical Problems in Engineering*, 2013, 8, 2013, pp.

[22] X. Shao, X. Dai, Z. Chen and X. He, Real-time 3D digital image correlation method and its application in human pulse monitoring, *Applied optics*, 55, 4, 2016, pp. 696-704.

[21] D. Zhang and D. D. Arola, Applications of digital image correlation to biological tissues, *Journal of biomedical optics*, 9, 4, 2004, pp. 691-9.

[23] M. Malesa, K. Malowany, L. Tyminska-Widmer, E. A. Kwiatkowska, M. Kujawińska, B. J. Rouba and P. Targowski, Application of Digital Image Correlation (DIC) for tracking deformations of paintings on canvas *Proc. of SPIE*, 8084, 2011, pp. 10.1117/12.889452.

[24] A. Polanczyk, M. Podyma, L. Stefanczyk, W. Szubert and I. Zbicinski, A 3D model of thrombus formation in a stent-graft after implantation in the abdominal aorta, *Journal of biomechanics*, 48, 3, 2015, pp. 425-31.

[25] A. Polanczyk, M. Podyma, L. Trebinski, J. Chrzastek, I. Zbicinski and L. Stefanczyk, A Novel Attempt to Standardize Results of CFD Simulations Basing on Spatial Configuration of Aortic Stent-Grafts, *PloS one*, 11, 4, 2016, pp. e0153332.

[32] J. Bergenholtz, J. Ulama and M. Zackrisson *Oskolkova*, Analysis of small-angle X-ray scattering data in the presence of significant instrumental smearing, *Journal of applied crystallography*, 49, Pt 1, 2016, pp. 47-54.

[33] Y. Wang, Z. Zhao and J. Wang, Microscopic vision *modeling* method by direct mapping analysis for micro-gripping system with stereo light microscope, *Micron*, 83, 2016, pp. 93-109.

[34] C. Duane and C. Brown, Decentering distortion *of* lenses., *Photometric Engineering*, 33, 3, 1966, pp. 444–462.